Science of the Total Environment 907 (2024) 167788

Contents lists available at ScienceDirect

Science of the Total Environment

journal homepage: www.elsevier.com/locate/scitotenv

An Arctic natural oil seep investigated from space to the seafloor

Giuliana Panieri [a,f,*], Claudio Argentino [a], Sofia P. Ramalho [b], Francesca Vulcano [c], Alessandra Savini [d], Luca Fallati [d], Trond Brekke [f], Giulia Galimberti [d], Federica Riva [d], João Balsa [b], Mari H. Eilertsen [c,e], Runar Stokke [c,e], Ida H. Steen [c,e], Diana Sahy [g], Dimitri Kalenitchenko [a,h], Stefan Büenz [a], Rune Mattingsdal [i]

[a] Department of Geosciences, UiT – The Arctic University of Norway, Tromsø, Norway
[b] Centre for Environmental and Marine Studies (CESAM) & Biology Department, University of Aveiro, Aveiro, Portugal
[c] Department of Biological Sciences, University of Bergen, Bergen, Norway
[d] Department of Earth and Environmental Sciences, University of Milano – Bicocca, Milano, Italy
[e] Centre for Deep Sea Research, University of Bergen, Bergen, Norway
[f] EXPLORO Geoservices, Trondheim, Norway
[g] British Geological Survey, Keyworth, Nottingham NG12 5GG, UK
[h] LIttoral ENvironnement et Sociétés (LIENSs), La Rochelle Université, Bâtiment ILE, La Rochelle, France
[i] Norwegian Petroleum Directorate, N-9407 Harstad, Norway

HIGHLIGHTS

- An active seep in the Arctic Ocean has been emitting oil since Late Pleistocene.
- Late Pleistocene ice melting unlocked hydrocarbons trapped beneath the ice shelf.
- Remote sensing and seafloor imagery revealed oil seep offshore Prins Karls Forland.

GRAPHICAL ABSTRACT

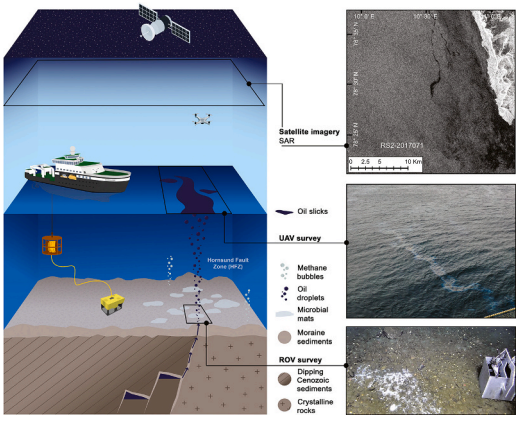

ARTICLE INFO

Editor: Jay Gan

Keywords:
Hydrocarbons
Methane
Prins Karls Forland

ABSTRACT

Due to climate change, decreasing ice cover and increasing industrial activities, Arctic marine ecosystems are expected to face higher levels of anthropogenic stress. To sustain healthy and productive ocean ecosystems, it is imperative to build baseline data to assess future climatic and environmental changes. Herein, a natural oil seep site offshore western Svalbard (Prins Karls Forland, PKF, 80–100 m water depth), discovered using satellite radar images, was investigated using an extensive multiscale and multisource geospatial dataset collected by satellite, aerial, floating, and underwater platforms. The investigated PKF seep area covers roughly a seafloor area of

* Corresponding author at: Department of Geosciences, UiT – The Arctic University of Norway, Tromsø, Norway.
E-mail address: giuliana.panieri@uit.no (G. Panieri).

https://doi.org/10.1016/j.scitotenv.2023.167788
Received 11 July 2023; Received in revised form 10 October 2023; Accepted 10 October 2023
Available online 19 October 2023

Baseline study
Carbonate
Microbial mats
Oil

30,000 m^2 and discharges oil from Tertiary or younger source rocks. Biomarker analyses confirm that the oil in the slicks on the sea surface and from the seep on the seafloor have the same origin. Uranium/Thorium dating of authigenic carbonate crusts indicated that the seep had emanated since the Late Pleistocene when ice sheet melting unlocked the hydrocarbons trapped beneath the ice. The faunal communities at the PKF seep are a mix of typical high latitude fauna and taxa adapted to reducing environments. Remarkably, the inhospitable oil-impregnated sediments were also colonized by abundant infaunal organisms. Altogether, in situ observations obtained at the site provide essential insights into the characteristics of high–latitude oil seeps and can be used as a natural laboratory for understanding the potential impacts of human oil discharge into the ocean.

1. Introduction

The adverse effects of oil pollution in marine environments are of great concern worldwide. Every year, millions of tons of oil, significantly underestimated in the past, enter the ocean mainly because of human activities (Dong et al., 2022) due to crude oil production, their use and transport, and accidental industrial spills. Nonetheless, natural flux of oil and methane gas are also found along the continental margin resulting from the degradation of organic matter in anoxic sediments (Barnes and Goldberg, 1976), released from geological reservoirs at hydrocarbon seeps (Du et al., 2014) and dissociating methane hydrate deposits (Panieri et al., 2017).

In the high-Arctic sea, extensive methane seepage areas have been discovered surrounding the Svalbard archipelago at shallow continental shelves and within the adjacent deep-sea (Panieri et al., 2017), on the East Siberian Arctic Shelf (Steinbach et al., 2021), and within the Canadian Arctic (Ishizawa et al., 2019). For most study sites, both in shallow and deep water, methane emissions have been suggested to result from gas hydrate dissociation enhanced over the last century by warming the Arctic Ocean bottom water (Serov et al., 2017) and glacial-isostatic adjustments occurring since the last deglaciation (Schneider et al., 2018; Dessandier et al., 2021) and beyond (Panieri et al., 2023). More recently, additional documented oil seeps from hydrocarbon reservoirs within the Barents Sea have been detected using satellite imagery (Mityagina and Lavrova, 2022; Serov et al., 2023). The PKF oil-dominated seep offshore western Svalbard was the first site to be discovered and sampled within the high-Arctic (Bünz and Panieri, 2021). The continental shelf west of PKF is 20–30 km wide at water depths between 50 and 250 m. A prominent moraine system, the Forlandet moraine complex, has dominated the seafloor along the shelf since the last glacial maximum, and radiocarbon dating of methane-derived authigenic carbonate indicates that seepage in the area has been active since the last deglaciation ~15 ky BP (Berndt et al., 2014).

As deep-sourced hydrocarbons migrate through the sedimentary column and reach the seafloor, they contribute to the formation of anoxic sediments and sustain specialized chemosynthesis-based ecosystems (Levin et al., 2016). While there is a substantial body of literature on fauna from gas seeps (Levin et al., 2016 and reference therein), our understanding of biological communities in oil-dominated seepage systems remains very limited (Leifer, 2019), with no prior characterization of such systems in the Arctic. The recent discovery of PKF natural oil seeps has unveiled a wealth of information with profound implications for this region. These occurrences, though seemingly inconspicuous, hold critical importance for our understanding of this unique ecosystem and can pave the way for valuable insights and conservation strategies knowing that the continuous ongoing loss of Arctic Sea ice has increased the prospect for Arctic resource exploitation such as fishing, extraction of oil, gas and minerals, tourism, which also opens for more trans-Arctic shipping (Gunnarsson, 2021). In addition, it has been shown that there are numerous analogous geological settings (areas that have experienced uplift and glacial erosion like PKF) across the North Atlantic and Arctic continental margins (Serov et al., 2023) that could potentially emit oil, impacting marine biology and ecology.

In this study, we have comprehensively characterized the geomorphology, origin, and discharge volume of hydrocarbons at the PKF site. Additionally, we conducted an in-depth investigation of the geochemistry of oil, pore water, and sediments and dated carbonate crusts. Furthermore, our research delved into the diverse biological communities near methane and oil seepages, encompassing microbial, meiofauna, macrofauna, and megafauna. Altogether, this study establishes a valuable baseline for future research endeavors in Arctic and worldwide oil seeps.

2. Materials and methods

2.1. Study design

The main objective of this study was to prove the existence of an oil seep site offshore PKF as identified from satellite images. Secondary objectives included defining the origin of oil and assessing its impact on Arctic biodiversity based on a comprehensive sampling that included oil, sediment, micro-meio-macro-megafauna from the oil seeping site and from an area of similar depth, and sediment type, but with no oil or methane seepage (see Graphical abstract). Once the seep was observed at the sea surface offshore western Svalbard, we planned an expedition that included a research vessel capable of deploying an ROV (Remotely Operated Vehicle) to collect sediment and biological samples.

The delay between the acquisition of satellite images and the expedition could have prevented us from exactly locating the seepage area. Such an issue was avoided by performing Uncrewed Aerial Vehicle (UAV) surveys within the study site. Once we located a zone where gas and methane bubbles were observed to burst, we commenced an ROV survey. During ROV dives, imagery and samples were obtained for various analyses to elucidate an integrated view of the oil seep (Fig. S2, Table S1). Video-guided sampling targeted microbial mats in areas where methane bubbles and oil droplets escaped. To avoid large-scale differences in observation associated with changes in the environmental setting, such as currents, suspended material, and food availability, reference samples were collected in relative proximity in area without seepage evidences.

2.2. Remote sensing

2.2.1. Satellite remote sensing for observing oil slicks on large scale

Since it allows the observation of vast areas unaffected by clouds, Synthetic Aperture Radar (SAR) satellite detection is commonly used for detecting and monitoring oil slicks (Alpers et al., 2017) (Migliaccio et al., 2015). SAR can detect oil slicks because slicks modify seawater viscosity, thus producing a strong impact that can be measured by SAR: backscatter is attenuated and oil slicks appear as a dark patch on SAR images (Lien et al., 2022) (Fiscella et al., 2000). Using weather-compliant satellite images from RADARSAT-2 and SENTINEL-1 satellites spanning from 2014 to 2021 (Fig. 1), a consistent oil slick origin was detected at coordinates 78°29.6′N, 10°31.5′E (Fig. 1).

2.2.2. Uncrewed Aerial Vehicles (UAVs) for local sea surface inspection

To locate the oil slick, we surveyed the area of interest, previously identified through the analysis of SAR data, using a consumer-grade UAV, equipped with a high-resolution RGB camera. For this purpose, we employed a DJI Mavic 2 Pro equipped with a 1" CMOS camera sensor

(20 MP) that can collect images with a resolution (R) of 5472 × 3648 pixels, and an integrated GPS/GLONASS system. We deployed the UAV from the deck of R/V Kronprins Haakon in May 2021 (Bünz and Panieri, 2021), to collect high resolution imagery data and video (i.e., at the centimeter level over an area of 0.1 km^2) by flying at an altitude from the sea surface of ca. 25 m. Oil slicks were detected from the point where oil droplets emerged at the sea surface to approximately 1 km downstream. This observation allowed for pinpointing the exact location of oil bubbles emission site on the sea surface, making it possible to deploy the ROV on that site.

2.2.3. ROV settings for underwater photogrammetric data acquisition and Structure from Motion (SfM) processing

The Ægir6000, a work-class ROV, equipped with two forward-looking (45° and 60°) cameras and one downward-looking HD video camera, filmed the seafloor along four, 100 m parallel transects that were spaced 2 m apart, at a constant speed (0.3 Knots) and altitude (2 m). Additional ROV surveys were performed to collect sediment and fauna samples. Accurate ROV positioning was based on Ultra-Short Base-Line (USBL) navigation, using a dead-reckoning based on an inertial navigation system complemented with a Doppler Velocity Log. Based on videos obtained from the nadiral camera, a frame every second was automatically extracted in order to apply Structure from Motion (SfM) using Agisoft Metashape® (Agisoft, 2018) following a well-established photogrammetric workflow (Fallati et al., 2020) (Lim et al., 2020) (Price et al., 2019). As a first step, video frames were aligned line by line using a high-accuracy setting, to generate a sparse point cloud. Once the photos were aligned, a detailed 3D Dense Point Cloud was generated. The scale of the models was computed using information obtained from two, parallel ROV laser beams, spaced at 14 cm. Laser spots on the frames were selected to determine the true distance between filmed objects. Scaled and georeferenced hyper-scale, three-dimensional (3D) landform models (i.e., Digital Terrain Models – DTMs) and orthomosaics were then created from the dense cloud. The models' spatial resolution was, respectively, 2 and 1 mm/pixel and supported the estimation of seafloor features and landforms associated with oil slicks.

2.2.4. Mega-epifauna annotation, habitat, and morphometric analyses

The identification and quantification of all mega-epifaunal, morphologically distinct taxa (designated as morphospecies), as well as microbial mats, were annotated in orthomosaics using the open-sourced software PAPARA(*ZZ*)I (Marcon and Purser, 2017). Mega-epifaunal abundances were expressed as individuals per m^2 (ind.m^2). Microbial mat patches were counted, the areal extension was measured on ROV-based photomosaics, and coverage was quantified using the average nearest neighbor analysis performed in ArcGIS® 10.8 software. The 3D Analyst Tools in ArcGIS were used to analyze the DTMs and orthomosaic models. Additionally, land surface parameters were computed and implemented in Trimble eCognition Developer 9.4. ® to

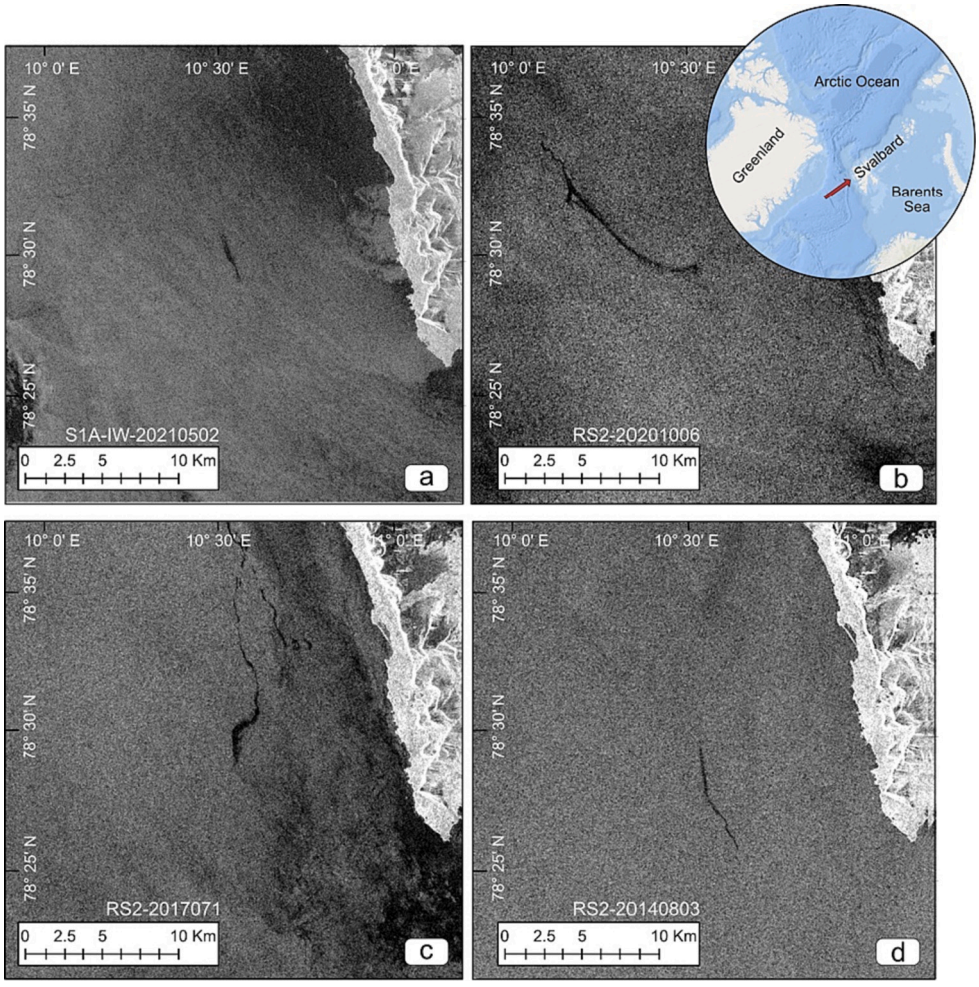

Fig. 1. Prins Karls Forland oil slick. Composite figure showing oil slicks from Synthetic Aperture Radar (SAR) images (a-d), The small round index map on the top right of the figure shows the Arctic Ocean, Svalbard, Greenland, and the Barents Sea. The red arrow is pointing toward the investigated area. The satellite images (a-d) are from Copernicus Sentinel data (2021). RADARSAT-2 Data and Products © MDA Geospatial Services Inc. (2014, 2017, 2020) – All Rights Reserved, provided by NOSA/KSAT. RADARSAT is an official mark of the Canadian Space Agency.

automate the recognition of microbial mats on the orthomosaics and detect spatial patterns at the seafloor through Object-Based Image Analysis (OBIA) (Table S2).

2.3. Oil sampling and geochemistry

The sampling of oil slicks at the sea surface was accomplished using a small boat equipped with a telescopic pole. Ethylene-TetraFluoroEthylene membrane (ETFE sheet) was attached to the end of the pole and placed onto the oil-stained sea surface. ETFE membranes encourage oil to be drawn from the sea surface. The oil then coats the membrane's surface. When repeatedly exposed to an oil sheen, a maximum amount of oil becomes coated on a membrane. Once good visual coverage of oil was achieved during sampling, oil coated membranes were placed into sample bottles and stored until further analysis. Oil samples were also extracted from sediment cores, as described in 2.5.

Geochemical analyses for all oil samples were performed at the laboratories of Applied Petroleum Technology (APT) in Oslo, Norway. All laboratory procedures follow NIGOGA, 4th Edition (Weiss et al., 2000), and include the following procedures/analytical conditions: 1) deasphaltening, 2) medium pressure liquid chromatography (MPLC), 3) the gas chromatography (GC) of the whole oil, 4) a GC analysis of the saturated fraction, 5) a gas chromatography–mass spectrometry (GC–MS) analysis of the saturated and aromatic fractions, 6) a GC–MS analysis of alkyl-benzenes, 7) a GC–MS/MS analysis of age-specific biomarkers, 8) a GC–MS analysis of the polar fraction, and 9) a GC–MS analysis of diamondoids within saturated fractions. The GC analysis of Extracted Organic Matter (EOM) is effectively equivalent to GC-WO (whole oil GC), although the most volatile components were inevitably lost during the extraction and concentration procedure. The C10+ range is; generally, little affected when care is taken not to evaporate extracts to dryness, as is performed at APT (e.g., the methylnaphthalene data is considered reliable).

The age-diagnostic biomarkers analysis provided clear constraints on the age of oil samples. The Nordiacholestane ratio (NDR), believed to originate from diatoms, radiated rapidly for the Cretaceous and Tertiary (Holba et al., 1998). An NDR above 0.25 indicates a post-Jurassic age, while values above 0.5 indicate a Tertiary or younger age. Oleanane originates from flowering land plants, and its presence in samples indicates a Cretaceous or younger age (Peters et al., 2005). Oleanane is commonly quantified using the Oleanane index. Values for oleanane above 0.0 indicate a post-Jurassic age, while values above 0.5 indicate a Tertiary or younger age.

2.4. Sediment sampling

Sediment samples for sediment and pore-water geochemistry studies, as well as biology investigations, were collected by push cores and blade coring using the Ægir6000 ROV deployed from the moon pole of the RV Kronprins Haakon. A total of five ROV guided push-cores were collected in microbial mats where methane and oil bubbles were escaping (PusC-01, PusC02, PusC03, PusC-05, and PusC-06) (Fig. S2). Three additional cores were taken, either by means of the push corer or blade corer (PusC-04, BlaC-01 and BlaC-02), in the vicinity without any evidence of seepage. The push coring device is composed of fiber glass, is 60 cm long, and has a diameter of 8 cm. The core liner was pushed into sediments using the ROV manipulator and then placed into the core holder. The blade corer frame is 32 cm long and can sample a volume of sediment with a larger rectangular area of approximately 25 × 10 cm. The blade corer automatically closes at the bottom to avoid sample loss. Push corer and blade corer liners are pre-drilled for pore water sampling and have a 1–2 cm resolution.

2.5. The geochemistry of pore fluids and oil-impacted sediments

Pore water samples were extracted from sediment cores using pre-wetted rhizons (0.15 μm mesh) and 12 mL-syringes attached to create a vacuum. Pore water samples were split into two aliquots: 1 mL was transferred into 1.5 mL glass micro-tubes for the dissolved inorganic carbon (DIC) analysis; 25 μL of mercuric chloride ($HgCl_2$) was then added to stop the microbial activity. Samples were then stored at 4 °C before analysis. The remaining pore water volume, ranging from 0.5 mL to 5 mL, was transferred into Eppendorf tubes and stored at −20 °C for sulfate analysis. The DIC isotopic composition was measured at UiB using a Thermo Scientific Delta V plus connected to a Gasbench II sample preparation unit. Results were corrected against the international carbonate standards NBS18 and NBS19 and in-house carbonate standards. Replicated analyses of standards yielded 1 SD better than 0.1 ‰. The sulfate concentration was measured via ion chromatography at TosLab in Tromsø (NO). Accuracy and precision were estimated based on repeated measurements of certified materials. The measured values agree within the uncertainty of the certified value. Analytical precision (relative standard error RSE) was 15 %. Bulk sediment samples (5 mL) were extracted from sediment cores for headspace gas analysis. Samples were extracted using a cut-off syringe and transferred into glass vials. For these samples, 5 mL of NaOH (1 M) was added, and samples were plugged with a rubber septum, sealed with aluminium crimp caps, shaken, and then stored at 4 °C prior to analysis. The headspace gas composition was measured using a ThermoScientific GC Trace 1310 GC–MS in the Stable Isotope Laboratory-SIL at UiT. The gas chromatograph system was calibrated using two external standards at 100 ppm and one standard at 1000 ppm. Gas bubbles were collected on the seafloor using a gas catcher on the ROV.

The carbon isotopic composition of hydrocarbon gas components was determined using a GC-C-IRMS system at ATP, Oslo. Aliquots were sampled using a Triplus RSH autosampler and analyzed on a Trace 1310 gas chromatograph (Thermo Fisher Scientific, MA, USA) equipped with a Poraplot Q column and a PTV (Programable Temperature Vaporizing) injector. The GC was interfaced via GC-Isolink II and Conflo IV to the Delta V Isotope Ratio Mass Spectrometer (IRMS) (Thermo Fisher Scientific, MA, USA). The reproducibility of $\delta^{13}C$ values in standards is better than 1 ‰ VPDB (2 s). The hydrogen isotopic composition of methane was determined using the GC-H-IRMS system.

Aliquots were sampled using a Triplus RSH autosampler and analyzed on a Trace 1310 gas chromatograph (Thermo Fisher Scientific, MA, USA) equipped with a Poraplot Q column and a PTV (Programable Temperature Vaporizing) injector. The GC was interfaced via GC-Isolink II and Conflo IV to the Delta V Isotope Ratio Mass Spectrometer (IRMS) (Thermo Fisher Scientific, MA, USA). Repeated analyses of standards indicate that the reproducibility of δD values is better than 10 ‰ VSMOW (2 s).

For sediment analyses, approximately 0.3 g of dry sediment was weighed into 10 mL Eppendorf tubes and decarbonated using 5 mL of 6 N HCl. Samples were rinsed five times with distilled water and dried at 50 °C. Analyses were performed using a Thermo-Fisher MAT253 IRMS coupled to a Flash HT Plus Elemental Analyzer hosted at the Stable Isotope Laboratory-SIL within the Department of Geosciences at the Arctic University of Tromsø. Duplicate samples were run throughout analyses and provided precision (1SD; $n = 12$) for TOC, TN, $\delta^{13}C_{org}$, and $\delta^{15}N$ better than 0.67 %, 0.007 %, 0.28 ‰ and 0.99 ‰ respectively. $\delta^{13}C$ and $\delta^{15}N$ were determined via normalization to international scales VPDB ($\delta^{13}C$) and Air-N_2 ($\delta^{15}N$) using three, in-house standards. The C/N atomic ratio was calculated using the atomic mass weighted ratio of TOC and TN as C/N = (TOC/12.011)/(TN/14.007).

2.6. Authigenic carbonate isotopic analyses ($\delta^{13}C$, $\delta^{18}O$, U/Th)

To observe microstructures and select target phases for isotope analyses and U/Th dating (Fig. 3), the carbonate concretion collected from the microbial mats (PusC-03) at 4 cmbsf was cut into thin sections. Two sub-samples were obtained via micro-drilling from matrix micrite and aragonitic cavity-filling cement. Following a reaction with anhydrous

phosphoric acid for 3 h at 50 °C, the stable isotope composition ($\delta^{13}C$, $\delta^{18}O$) was measured on a Thermo Scientific Gasbench II coupled to a Finnigan MAT 253 triple collector isotope ratio mass spectrometer at the Stable Isotope Lab-SIL, at UiT. Data are reported in ‰ notation relative to VPDB. The analytical error was better than 0.1 ‰ (1SD) for both carbon and oxygen.

Uranium and Thorium were measured on a Thermo Neptune Plus multi-collector inductively coupled plasma-mass spectrometer (ICP-MS) using a ^{236}U—^{229}Th isotopic tracer at the British Geological Survey, Geochronology and Tracers Facility (UK). Instrument parameters were monitored using CRM112a and IRMM3636 uranium and an in-house ^{229}Th-^{230}Th-^{232}Th reference solution as bracketing standards. Based on values reported by Cremiere et al. (2016) for background sediment samples obtained from a similar water depth range as for those in our study, a correction for initial detrital/hydrogenous ^{230}Th was applied.

2.7. Biology

2.7.1. Microbes (DNA sequencing and phylogenetic analyses)

Genomic DNA was extracted from sediment samples collected from a white circular microbial mat (diameter 20 cm, PusC-01) (Fig. S2). The resulting 28 cm-long core was sampled every 2 cm to 8 cmbsf, every 4 cm to 12 cmbsf, and every 8 cm to 28 cmbsf. Total DNA was extracted, based on manufacturer instructions, from 500 mg of sediment using a FastDNA™ SPIN Kit for Soil (MP Biomedicals, Santa Ana, CA, USA). The resulting DNA concentrations (Qubit Fluorometric Quantification – HS; Thermo Fisher Scientific, MA, UA) decreased from 156–57 ng μL^{-1} within the upper 8 cm of the core to 13–5.6 ng μL^{-1} from 8 to 28 cmbsf. DNA was sequenced at the Norwegian Sequencing Center (NSC) in Oslo, using an Illumina Novaseq 6000 sequencer and S4 reagents.

The taxonomic composition and abundance of resulting metagenomes were assessed using the assembly of SSU rRNA sequences using phyloFlash (Gruber-Vodicka et al., 2019). Computations associated with taxonomic classifications were performed on resources provided by Sigma2 - the National Infrastructure for High Performance Computing and Data Storage in Norway.

2.7.2. Sediment meiofauna and macrofauna

The sediment infauna investigated, including living benthic foraminifera (> 63 μm), metazoan meiofauna (> 32 μm) and macrofauna (> 1 mm) was recovered from sediments in three push cores taken from microbial mats, and two blade cores recovered in nearby areas without visible microbial mats or an indication of the presence of methane or oil (Fig. S2 and Table S1 for sample metadata). Visible macrofauna was picked from the sediment surface of blade cores and fixed in 96 % ethanol. Once the pore-water extraction was complete, each liner was sliced into five sediment depth layers and fixed in formaldehyde (4 %) seawater solution for morphological analyses. The remaining sediments were sliced every cm and preserved in plastic bags for the subsequent stable isotope geochemistry analysis of foraminifera.

In the laboratory, meiofauna was extracted from sediments using a density gradient solution in a centrifugation technique (Heip et al., 1985). Fixed samples were rinsed through 32 μm and 1 mm mesh sieves. The fraction retained within the 1 mm sieve was immediately transferred to 96 % ethanol for macrofauna sorting and identification. The retained sediment fraction (32 μm - 1 mm) was further washed and centrifuged three times using a colloidal silica polymer LUDOX HS-40 (specific gravity 1.19). The supernatant of each washing cycle was, again, collected using a 32 μm sieve. Following extraction and before investigations of living foraminifera and metazoan meiofauna, samples were kept in a buffered, 4 % formalin and stained with Rose Bengal. All organisms were counted and classified under a stereomicroscope to higher taxon levels (e.g., following (Higgins and Thiel, 1988). Nematodes and benthic foraminifera, the dominant meiofauna taxa, were further investigated for the 0–1 cm sediment fraction. Whenever possible, identifications were conducted to the genus level. In total, 150 nematodes were randomly picked from each replicate and mounted on permanent glycerin slides following stepwise dehydration in a graded series of ethanol: glycerin mixtures (Seinhorst, 1959). Nematodes were then identified under the microscope down to the lowest possible taxonomic level (i.e., genus or species) using pictorial keys (Platt and Warwick, 1988; Warwick et al., 1998) and literature available within the Nemys Database (Bezerra et al., 2022). Living foraminifera were classified at the genus level according to (Alfred R. Loeblich, 1988). A more detailed investigation into these groups is currently ongoing.

Macrofaunal samples were identified at the family or genus level at the University of Bergen (Norway) using a Leica MZ8 stereomicroscope, with assistance from taxonomic experts at the University Museum of Bergen. This study only identified macrofauna to the family or genus level. However, further investigations are planned, including molecular analyses designed to understand better the degree of specialization in fauna and overlap with other regional reducing environments.

3. Results

3.1. Remote sensing observations

An analysis of multiple SAR satellite images from 2014 revealed persistent oil slicks on the sea surface, 10 km offshore of PKF (Fig. 1), located at approximately 78°29.6′ N, 10°31.5′ E with an uncertainty margin of approximately ±300 m. Due to surface currents and wind conditions, the surface slicks' shape, dimension, and orientation varied over time.

In May 2021, the CAGE21-1 research expedition on board the R/V Kronprins Haakon conducted an on-site investigation, corroborating the presence of surface slicks (Fig. 1). The slicks exhibited dimensions ranging from 0.1 to 10 km in length and 0.2 to 1 km in width, discernible as distinct striations on the sea surface when observed from both the research vessel and unmanned aerial vehicles (drones) (Fig. 1) and varied in the area from 1 to 6 square km. These observations were made under favorable weather conditions characterized by calm winds and no waves. During our expedition, the absence of other ships around R/V Kronprins Haakon excludes the possibility that the oil slicks were emitted from ship engine operations. The fate of bubbles from seeps and their impact strongly depends on bubble size and seabed depth (Leifer, 2019). Bigger and shallower bubbles (Leifer and Patro, 2002) and oily bubbles (MacDonald et al., 2002) are more likely to reach the wave-mixed layer and sea surface. Water column dissolution and current drift are minimal for shallow oil seepage like PKF oil seeps at ca 100 m water depth. Therefore, the oil arrives at the sea surface in a narrow surfacing area and forms a slick with a similar composition to when it was released.

The total volume of oil in a slick depends on the oil layer's thickness. The Bonn Agreement Oil Appearance Code (BAOAC; (Lewis, 2007)) estimates the thickness of an oil layer based on the appearance of oil at the sea surface. The observed oil slick from the ship during the expedition had a silvery/grey appearance. However, when oil droplets emerged at the sea surface, rainbow colours were also observed. These results correspond to BAOAC values for oil droplets of 0.04–0.3 μm and 0.3–5.0 μm, respectively. Based on these observations and using the same assumptions as Garcia-Pineda et al. (2013), the majority of slicks (95 %) in the area are ~0.1 μm in thickness, while fresh oils (5 %) are ~1 μm in thickness. Using these values and considering a 24-h life span for slicks, we calculated a discharge volume to the sea surface of 3.7 barrels of oil per day (588 L day^{-1}) for a 1 km^2 slick and 22.5 barrels of oil per day (3578 L day^{-1}) for a 6 km^2 slick the latter being representative of slicks observed under favorable meteorological conditions characterized by calm winds and negligible wave action.

3.2. Seafloor geomorphology and ROV-based observation, mapping and sampling

The hydrocarbon seepage phenomena on the seafloor on the continental shelf west of PKF island appear to be influenced by the geological settings. The seepages correspond with distinctive assemblies of ice-marginal submarine landforms documenting the Pliocene-Pleistocene advance and ice retreat across the west PKF margin (Ottesen et al., 2008). From 10 to 20 km directly west of PKF there is a pronounced ridge system, with a crest at about 90 m water depth, known as the Forlandet Moraine Complex (FMC) (Ottesen et al., 2008). A seismic section crossing our study area (Fig. 2C in (Landvik et al., 2005)) shows bedrock with westward dipping clinoforms covered by a thin (<10 m) veneer of glacial and marine sediments (i.e. moraine ridges) that form a series of trough and ridge morphology above a major unconformity. In addition to moraine ridges, sub-circular or slightly NW-SE elongated depressions, up to 6–10 km in diameter and 100 m deep, occur to the east of the forlandet moraine complex, interpreted as glaciotectonic landforms (i.e., glaciotectonic detachment of larger blocks of sediments, incorporated in the ridge) (Ottesen et al., 2008). However, detailed information on the tectonic activity in the region and its potential influence on the submarine domain are still incomplete and limited to a major NS-oriented fault zone that marks the transition zone between westward dipping Cenozoic sediments and older basement rocks. Our ROV visual observations revealed that the PKF oil seepage site encompassed an approximate area of 30,000 m^2 along the sloping southwestern edge of a moraine ridge (Fig. S1). However, it is highly likely that the seepage area extends well beyond our observed boundaries. The seafloor consisted of a mixed substrate, primarily made by pebbles, cobbles to boulder-sized rocks identified as glacial till and disarticulated bivalve shells; finer-grained sediment was locally observed toward more depressed areas in small-scale spots or filling the space between coarser-grained clasts and rocks, indicating remobilization under strong bottom current. The cobble to boulder-sized rocks are substrates of numerous anemones, polychaetes, and other organisms, better described in Chapter 3.5. The white patches of microbial mats (family *Sulfurovaceae*) appeared circular or elongated (ca 30–50 cm in length; Fig. 2) when in clusters, often exhibiting streams of methane bubbles and oil droplets. In a photomosaic survey of an area of ~720 m^2 (Table S1, including data from 2 expeditions, CAGE21–1 (Bünz and Panieri, 2021) and CAGE22-2 (Panieri et al., 2022), we counted 75 microbial mat patches that cover 3.6 m^2 in total (~10 patches per 100 m^2 with a surface area of, on average, 0.06 m^2; Table S2). It is interesting to note that the patches appear to be aligned in a southeast to northwest direction (Fig. 2). During the ROV survey, we noticed that the ascent of methane bubbles through the water column was rapid compared to the rising speed of oil droplets. Oil droplets are brown in color, and while rising, their shape changes from a spherical shape to a gradually increasing oblate disk-like shape. This disk-like shape can explain the lower average rising speed, combined with oil's low buoyancy (compared to gas). With the ROV manipulator, we collected push and blade cores for sediment geochemistry, pore water extractions, and biological analyses from patches of microbial mat habitats and two reference sites with no evidence of seeping methane or oil (Figs. S1 and S3).

3.3. Oil geochemistry

To determine the compositional linkages between sea surface oil slick and seafloor seeping oil both oils were analyzed and geochemically correlated (Figs. S3, S4 and S6). The analysis of bulk oil extracts revealed hydrocarbons occurring in variable proportions. Slicks and seafloor seeping oil showed a significant amount of Unresolved Complex Mixture (UCM) often seen in biodegraded oil. The UCM of the slicks was overprinted by a peculiar n-alkane pattern, where all odd-numbered n-alkanes were missing. To the best of our knowledge, such a pattern has never been reported in petroleum, and it cannot be caused by biodegradation since biodegradation would remove all n-alkanes without preference (Wenger et al., 2002). We do not have any explanation for the odd-numbered n-alkanes missing in our samples. However, isotope analyses of the aromatic and saturate fractions evidenced values consistent with petroleum.

Slicks and seafloor seeping oil contain practically identical

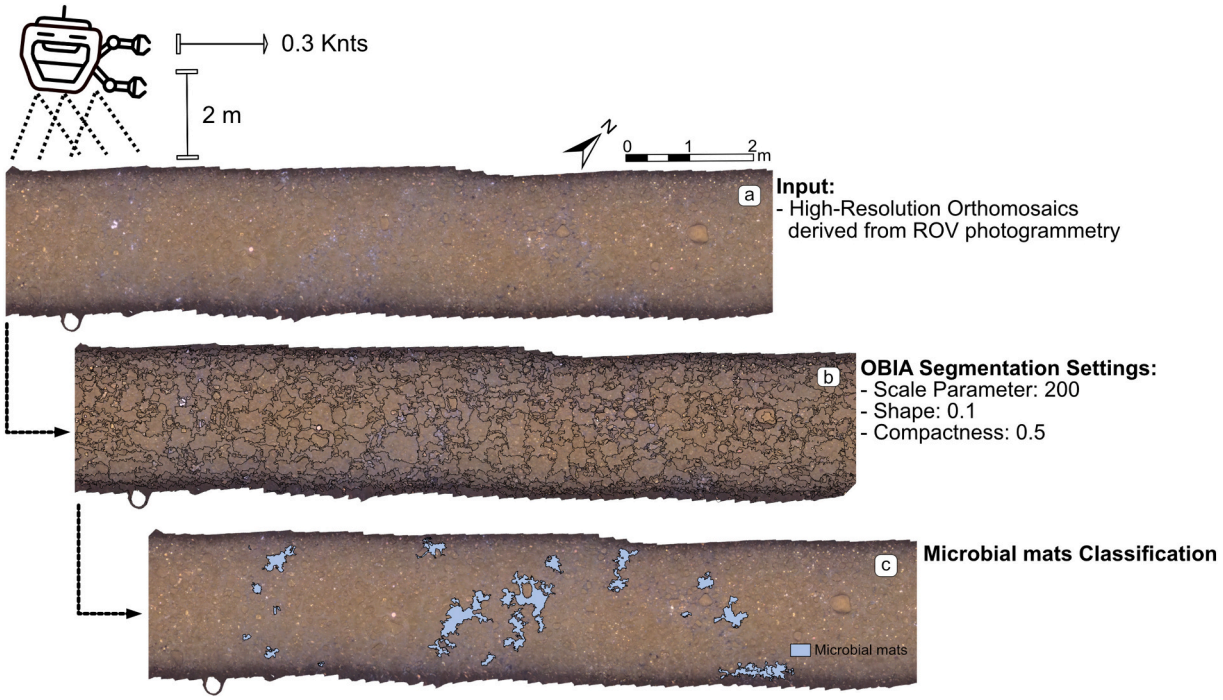

Fig. 2. A segment of the seafloor ROV orthomosaic. The figure illustrates a portion of high-resolution orthomosaic created by high-resolution imagery collected along a single ROV transect, with visible patches of microbial mats with a preferential southeast to northwest direction. Similar imagery was used for mega-epifauna recognition and classification (a), processed with eCognition multiresolution segmentation algorithm (b) for the identification of bacterial mats patches (c).

biomarker fingerprints for petroleum (Figs. S3). Age-diagnostic biomarkers prove this oil to be a rare type of petroleum, different from the known Triassic and Late Jurassic oils in the Barents Sea (Fig. S4). From the results, we conclude that oil in the slicks on the surface derives from source rocks located deeper than the glacial deposits.

Using a well-known general scheme for hydrocarbon biodegradation (Head et al., 2003), PKF samples revealed the following biodegradation signs: 1) a large UCM, very often due to bio-resistant compounds accumulating over periods of biodegradation; 2) erratic values for maturity biomarker ratios; and 3) the presence of 25norHopanes. Two very resistant ratios, namely %27Ts and %ββ, were consistent in our samples. Based on %27Ts and %ββ biomarkers, slick and seep oil had almost identical maturities, corresponding to an early-middle oil window (%Ro = ca 0.6–0.7 in source rock).

Age-diagnostic biomarkers yielded explicit constraints on the age of oil samples, which is Tertiary or younger (Fig. S4), with an NDR ratio close to 0.68 and an Oleanane index close to 0.6. Nordiacholestanes likely originate from diatoms, which radiated rapidly in the Cretaceous and Tertiary periods in the region (Holba et al., 1998).

3.4. Sediment geochemistry

3.4.1. Pore water and gas

Sulfate concentration profiles in sediment cores from microbial mats emitting oil and gas displayed intense sulfate reduction close to the seafloor associated with anaerobic methane oxidation (AOM) (Table S3, Fig. 3), defining a Sulfate-Methane Transition Zone (SMTZ) at 10 cm. The $\delta^{13}C$ composition of Dissolved Inorganic Carbon (DIC) was consistently above 0 ‰, with an evident increasing downward trend (maximum value of +33.5 ‰ at 12 cm in PusC-02, Fig. 3). Such elevated isotopic values are typically found in the methanogenic zone of the sediment, where the preferential microbial utilisation of isotopically lighter molecules leads to a progressive enrichment in ^{13}C in the residual carbon substrate (Whiticar, 1999). Therefore, we suggest that DIC values in seep-impacted cores reflect the advection of fluids from a depleted methanogenic carbon pool. The reference site (within the seepage area, but with no evidence of hydrocarbon seepage in oil and gas streams or microbial mats) displayed a gentle sulfate gradient and DIC values reflecting a mix of seawater DIC ($\delta^{13}Csw \sim 0$ ‰) and DIC from organic matter mineralisation (-26 ‰ $< \delta\ ^{13}C_{TOC} < -21$ ‰), typical of normal marine environments. The isotopic composition of seeping gas bubbles was characterized by a $\delta^{13}C_{CH4} = -48.4$ ‰, a $\delta D\text{-}CH_4 = -196$ ‰, and a $\delta^{13}C_{CO2} = 19.9$ ‰ (Fig. S6), indicating a dominant thermogenic component affected by biodegradation (Milkov and Etiope, 2018), in agreement with results obtained from oil geochemistry analyses.

3.4.2. Carbon-nitrogen geochemistry

The total organic carbon content in sediment cores from microbial mats emitting oil and gas ranged from 1.4 to 6.1 %, whereas at the reference site, the highest values were 2.1 and 0.7 % (Fig. S5, Table S3). C/N ratios displayed clear differences between the two habitats. The C/N atomic ratios in marine sediments reflect a mix of different proportions of marine organic matter (MOM) with a $C/N < 10$ and terrestrial organic matter (TOM) with a $C/N > 20$ (Perdue and Koprivnjak, 2007). Bulk organic carbon and C/N ratios in oil seep-impacted sediments generally increase with oil content generating $C/N > 50$ (LaMontagne et al., 2004). reflecting the preferential microbial utilisation of nitrogen-rich compounds during diagenesis of organic matter (Altabet, 2005). Therefore, the observed high TOC and C/N ratios in the seep site with microbial mats are interpreted to reflect oil impregnation. The addition of microbial biomass linked to the presence of oil in the sediment likely influenced the stable carbon and nitrogen isotopic composition of the sediment, toward lower $\delta^{13}C_{TOC}$ and $\delta^{15}N_{TN}$ compared to the reference site (Lehmann et al., 2002) and highly scattered throughout the cores (Fig. S5).

3.4.3. Authigenic carbonates

An authigenic carbonate concretion was collected from a microbial mat at 4 cmbsf. It exhibited $\delta^{13}C$ values of -28.7 ‰ for the micrite phase and -26.0 ‰ for the isopachous cement (Fig. 3). A carbonate forming only from bicarbonate released by anaerobic oxidation of methane having $\delta^{13}C = -48.4$ ‰ would show a $\delta^{13}C = -57.4$ ‰ (considering fractionation during AOM of ~9 ‰ (Altabet, 2005)). Still, admixture of heavier DIC from seawater and organic matter degradation tends to result in a carbonate $\delta^{13}C$ lower than approximately -30 ‰. If oil were the only alkalinity source in pore waters, the carbonate $\delta\ ^{13}C$ would be similar to the one of the oil, which at this site ranges between -29.7 ‰ and -25.6 ‰. Therefore, the measured values demonstrate the presence of anaerobic oxidation of methane and oil. It is impossible to decipher the contribution of the two sources as it would require more geochemical constraints. Uranium/Thorium (U/Th) dating of carbonate cement

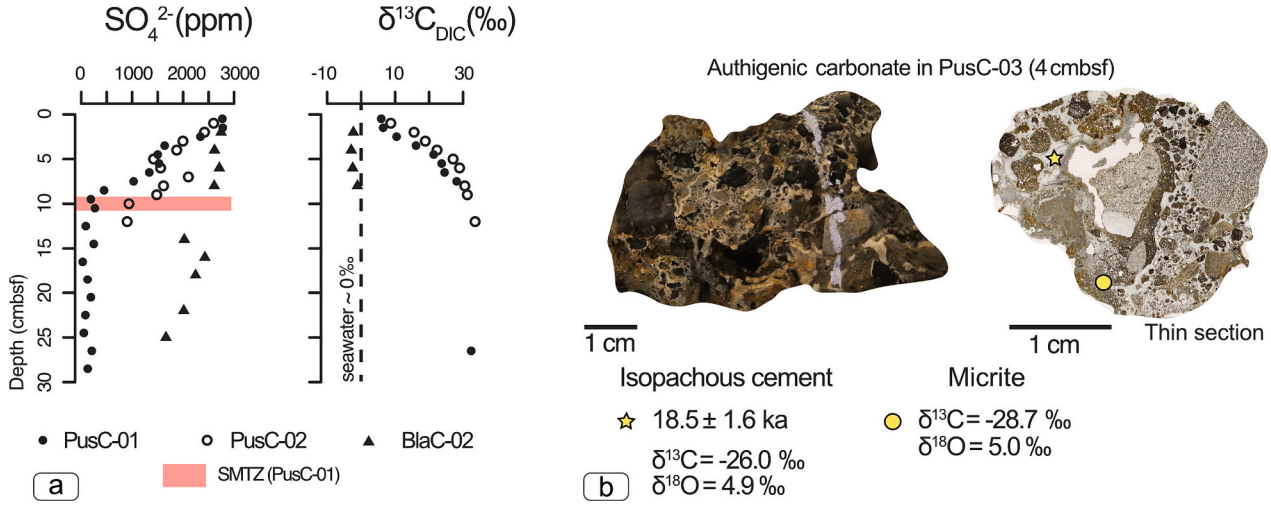

Fig. 3. Geochemical evidence of modern and past hydrocarbon seepage. (A) Pore water geochemistry of oil-charged sediments (PusC-01, PusC-02) from a microbial mat and reference core (BlaC-02). The sulfate-methane transition zone (SMTZ) in PusC-01 (marked with a transparent red area) was defined based on the sulfate vertical concentration profile (see methods for details). (B) An authigenic carbonate concretion found in PusC-03 (left) and its thin section (right) showing where the stable isotope geochemistry (yellow dot) and U/Th dating (yellow star) were performed. The age of the cement and the stable isotopes of the cement and and micrite are indicated.

yielded an age of 18.5 ± 1.6 ka, indicating protracted activity for this seepage system since the Late Pleistocene, soon after the Last Glacial Maximum, ~20 ka. The oxygen isotopic composition of carbonate phases yielded $\delta^{18}O$ values of 5.0 ‰ (micrite) and 4.9 ‰ (cement), pointing to formation in isotopic equilibrium with coeval cold bottom waters (Kim et al., 2007).

3.5. Biology

3.5.1. Microbial mats

When the sediment microbial community below a patch of the microbial mat was examined with PhyloFlash (Fig. S7) a remarkable transition in the community structure, particularly from the sediment-water interface to the lower sediment layers, was observed. At the sediment-water interface (0–2 cmbsf), sulfur-oxidizers within the Epsilonproteobacteria, order Campylobacteriota, family *Sulfurovaceae* represented the most abundant bacterial group (9 % relative abundance, rel. ab.), followed by Cyanobacteria. Gammaproteobacteria of the orders Beggiatoales and Methylococcales taking part in oxygen-mediated sulfur oxidation and aerobic methane oxidation were found in 3 % and 5 % rel. ab., respectively. Desulfobacterota of the orders Desulfobulbales/Dissulfuribacterales were detected in similar abundances. The

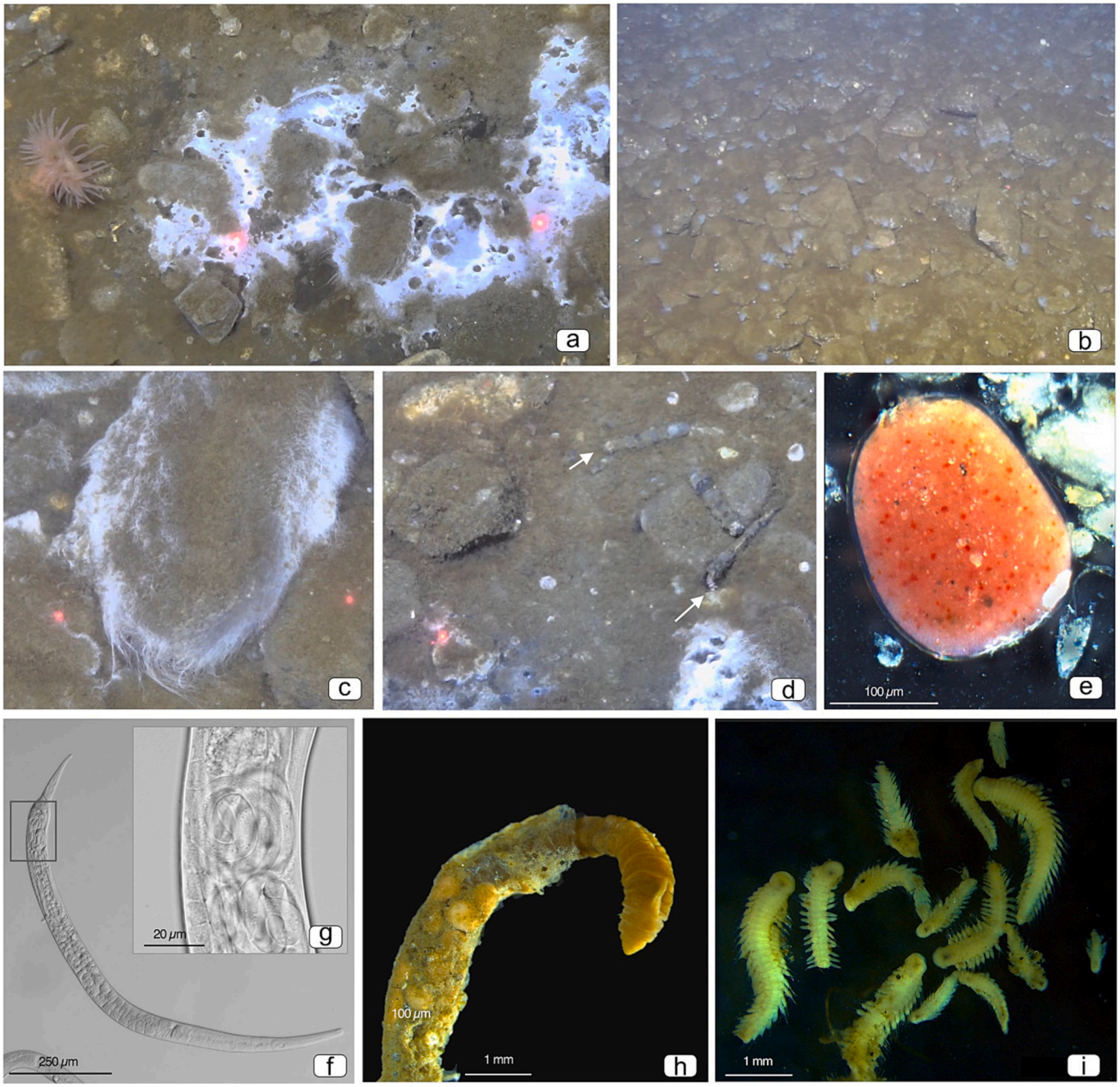

Fig. 4. Typical fauna observed above and within the sediment at the Prins Karls Foreland oil seep. Detailed ROV imagery of seafloor where filamentous bacterial mats were present with evidence of oil droplets and methane bubbles seeping (A, C) and commonly associated mega-epifauna taxa such as Actiniarians (A, B and C) and large Onuphidae polychaetes (*Nothria* sp.; white arrows in D). Among the sediment infauna in oil-impregnated sediments, examples include Monothalamids foraminifera (E). One of the most observed nematode species from the Monhysteridae family (F), presents a rarely seen ovoviviparous reproduction (G); and two of the most abundant macrofauna polychaetes from the families Capitellidae, *Capitella* sp. (H) and Dorvilleidae, *Ophryotrocha* sp. (I). ROV laser points (red dots in A, C, and D) distance is 14 cm.

archaeal population in the microbial mat was dominated by ANME-1b (8 % rel. ab.) and ANME-2c (3 % rel.ab.). The microbial community changed dramatically below the sediment-water interface from 2 to 8 cmbsf and became dominated by ANMEs, Dissulfuribacterales and *Candidatus* Atribacteria JS1 (~10 % rel. ab.). Below 8 cmbsf, the relative abundance of ANME-1b and Ca. Atribacteria JS1 increased (up to 50–70 % rel. ab.), while ANME-2c and Dissulfuribacterales abruptly disappeared. *Desulfosarcinaceae*, absent from shallower horizons, were detected between 8 and 20 cmbsf, reaching up to 15 % rel. ab. A small population of Lokiarchaeia and Pirellulaceae inhabited the sediments between 12 and 20 cmbsf, while Caldisericaceae appeared below 20 cmsbf. Our analysis also revealed that the sediment-water interface hosted marine Eukaryotes, such as Diatomea and Opisthokonta, representing approximately 12 % of the total assembled SSU sequences.

3.5.2. Sediment infauna

We identified infauna inhabiting microbial mats and reference sites, revealing that Nematoda constituted the most abundant taxon, followed by Harpacticoida copepods and their nauplii larvae, as well as Polychaeta and Foraminifera (Fig. 4). Total infauna abundance showed no significant differences between microbial mats and reference samples, but reference samples displayed greater diversity, containing typical taxa from the shelf area off Svalbard (Zajączkowski et al., 2010; Pitusi et al., 2021). In contrast, infauna communities from microbial mats had lower taxa richness despite high abundances, with specialized taxa dominating and thriving in reducing environments (see Table S4 for a taxon overview).

Among nematodes, the community was primarily represented by a single nematode species belonging to the Chromadoridae family, followed by a Monhysteridae species (*Halomonhystera disjuncta*), and a Linhomoeidae nematode species. Some nematode species exhibited ovoviviparity, suggesting that these organisms have developed adaptations to survive in toxic conditions within bacterial mat sediments rich in hydrogen sulfide and oil (Fig. 3).

Among living foraminifera (identified by Rose Bengal staining), monothalamids predominated in all samples, with porcelaneous and agglutinated species being rare. The agglutinated species are absent in the samples from microbial mats. We observed organic linings resembling Rotaliaceae (*Ammonia* sp. or *Elphidium* sp.) and possibly agglutinated foraminifera (Boonstra et al., 2015) in all samples.

Polychaete communities in bacterial mats were dominated by the families Capitellidae (*Capitella* sp.) and Dorvilleidae (*Ophryotrocha* sp.), with a few Siboglinidae. The siboglinids were small, thin, light brown tubes without the visible transverse rings typical for the genus *Oligobrachia*. Extracting worms from tubes following fixation was impossible, hindering further identification. However, tube morphology and the depths where specimens were collected suggest that they could belong to the genera *Siboglinum* or *Sclerolinum*. Another possibility is juvenile *Oligobrachia*, which sometimes lacks transverse rings on tubes (Sen et al., 2020). Capitellidae, Dorvellidae, and Siboglinidae are typically found in sulphidic sediments within hydrothermal vents, cold seeps, and organically enriched sediments in shallower waters (Holte and Oug, 1996). The macrofauna of reference samples consisted of typical taxa found in shelf areas off Svalbard (see Table S4) (Parapar et al., 2011).

3.5.3. Mega-epifauna

In total, 22 different taxa of mega-epifaunal organisms were observed inhabiting the area, and most are commonly found in other areas of the region at similar depths (Table S4). The most abundant taxa were polychaetes in the order Sabellida (feather duster worms; Fig. 4), a group that was generally sparsely distributed within the area except for a few exceptions that displayed large aggregations near microbial mats. The feather duster worms accounted for >40 % of total epifauna observations in photomosaics and reached densities up to 118 ind/m^2. Since both Sabellidae and Serpulidae were recovered in our samples, the aggregations likely included worms from both taxa. However, since tubes are generally invisible, separating them in the photomosaic was impossible. In areas with more extensive coverage of microbial mats, the most observed taxa were actiniarians, polychaetes from the family Onuphidae (*Nothria* sp., identified to the genus level based on sampled individuals), small sponges, and unidentified ophiuroids, as well as fish from the family Stichaeidae.

4. Discussion

4.1. Long-lasting oil seep driven by sub-seafloor geology

The release of hydrocarbons in the high Arctic is a known phenomenon (Andreassen et al., 2017; Panieri et al., 2017; Serov et al., 2017), yet, oil seeps have only recently been observed in areas that have experienced uplift and glacial erosion (Ivanov, 2019; Pavel Serov et al., 2022). Here we present the first multidisciplinary characterization of an oil seep on the Arctic shelf near Svalbard, unveiling a wealth of information with profound implications for our understanding of hydrocarbon dynamics in this region and its impact on the Arctic biota.

Longstanding shallow seismic data indicate that the seepage area offshore Prins Karl Forland appears to occur along the the Hornsund fault system within the transition zone between westward dipping Cenozoic sediments and older basement crystalline rocks, where the glacial till of the FMC is thinner (i.e., estimated to be <10 m). ROV photomosaic showing the apparent clustering of the microbial patches on the seafloor and their preferential alignment (Fig. 2), suggests that hydrocarbons are emitted from fractures aligned as the Hornsund fault system along a South-East to North-West direction (see Graphical abstract).

Geochemical analyses concluded that the seafloor and sea surface oil share the same source, originating from severely biodegraded petroleum with a thermal maturity indicative of the mid-oil-window stage of Tertiary period or younger (< 65 Ma), potentially derived from the Arctic Azolla blooms during the Eocene epoch (Speelman et al., 2009) or organic-rich sediments deposited during the Miocene (Knies and Mann, 2002). Subsequently, high geothermal gradients along the mid-Ocean Ridge, which is <100 km west of the PKF oil seep, could have accelerated the maturation of young source rocks and expedited the migration up-dip toward the Svalbard margin through a major system of faults and fractures (Knies et al., 2018). Notably, no prior report of oil with such a young geological origin has been reported within this specific sector of the Arctic or the broader North Atlantic region.

The question of where the biodegradation of the PKF oil primarily occurs, at the seafloor or is inherited from somewhere in the migration route, remains unresolved since our data can support both scenarios, and does not conflict with either. Yet, given that biodegradation takes time, PKF is an active seep, and the oil probably has only a short residence time within the seafloor sediments, it is probable that biodegradation occurs in a trap within the migration route. Likewise, the gas isotopic composition of seeping bubbles (with $\delta^{13}C_{CH4} = -48.4$ ‰, a $\delta D\text{-}CH_4 = -196$ ‰, and a $\delta^{13}C_{CO2} = 19.9$ ‰) (Fig. S6) indicate a predominant thermogenic component affected by biodegradation (Milkov and Etiope, 2018).

Considering the rate of discharge calculated from SAR satellite images, a range from 3.7 to 22.5 barrels of oil per day (588–3578 $Lday^{-1}$) may be discharged. Assuming this rate is representative of a constant daily rate throughout the year, 1350–8200 barrels (215,000–1,300,000 L) of oil per year may be discharged to sea at this seep site. This corresponds to ~1200 t/y rate, which is 0.08 % of all estimated natural oil emissions in the ocean (Kvenvolden and Cooper, 2003). The rate appears to be minor, but if we consider that U/Th datings of authigenic carbonates from PKF indicate that this seep has been active since 18.5 ka BP, then the amount of oil emitted into the environment becomes significant: 25–150 million barrels (using the same discharge rates as previously calculated and assuming a constant seep rate since the last glaciation).

4.2. Impact of natural oil seeps on Arctic sediment biogeochemistry and microbial communities

The PKF oil seep site shows high organic content (TOC), ranging from 1.5 to 6 %, with an increasing trend toward the seafloor. Such values are much higher when compared to those commonly observed in Arctic environments (1 % on average (Knies and Martinez, 2009)) and at our reference site, suggesting that prolific microbial mats observed at the seafloor contribute to the high organic content. Microbial analysis reveals a prevalence of chemosynthetic and heterotrophic microorganisms commonly found in hydrocarbon seeps (Emil Ruff, 2020; Stokke et al., 2012). These include aerobic and anaerobic methane oxidizers (Methylococcales and ANMEs), sulfur oxidizers (Beggiatoales), sulfate reducers (*Desulfosarcinaceae* and *Desulfobulbaceae*), and heterotrophic Ca. Atribacteria and Ca. Lokiarchaeota (Fig. S7). The presence of ANME groups and sulfate-reducing bacteria within the first few centimeters is consistent with the pore water results (Fig. 3) and suggests that methane is actively consumed by anaerobic methane oxidation (AOM) close to the sediment-water interface. The microbes-mediated degradation of methane is confirmed by the gas isotopic composition of seeping bubbles, in agreement with results obtained from oil geochemistry analyses (Fig. S6). The high sulfide fluxes released by AOM sustain the microbial activity of surface sulfur-oxidizing Epsilon- and Gammaproteobacteria. The observation of methane bubbles rising from patches of microbial mats indicated that part of the methane bypasses the biological filter at the SMTZ (located at 10 cm). This is likely due to high methane flow rates, also observed during ROV video surveys.

In addition to methane-degraders, the oil seep sediments were also inhabited by taxa that could participate in oil degradation. Ca. Atribacteria JS1 has often been observed in hydrocarbon seeps within the Guaymas Basin (20), in the Gulf of Mexico (Vigneron et al., 2017), in the high–latitude methane seeps at Nyegga (Pachiadaki et al., 2011), and oil reservoirs (Hu et al., 2020). Even though Ca. Atribacteria are described as organic acids fermenters, a partial pathway for the conversion of alkanes to acyl-CoA was identified in the genomes of Ca. Atribacteria JS1 (Liu et al., 2019), supporting their possible role in oil degradation at the PKF oil seep. The capacity to degrade long-chain hydrocarbons is well-known for members of the genus *Desulfosarcina* (Rabus et al., 2016). These were detected in high abundances below 8 cmbsf, suggesting that they could also take part in oil degradation at the PKF oil seep.

4.3. Faunal communities thrive in oil impacted habitats

Cold seep environments present unique challenges for seafloor organisms, especially when permeated with toxic compounds from crude oil. The faunal communities at PKF oil seep consist of a mix of typical high-latitude species and those specialized for reducing environments. Mega-epifaunal communities observed in imagery mainly showed taxa found in non-seep Arctic regions at similar water depth (Bergmann et al., 2011; Sahling et al., 2014; Sen et al., 2020). Notably, there is a distinct absence of visible tubeworm aggregations of Siboglinidae at PKF, with only a few small siboglinid worms found in the infauna. Siboglinids have been observed at all other Arctic seep sites (Gebruk et al., 2003; Panieri et al., 2017; Savvichev et al., 2018; Sen et al., 2020) and Oligobranchia is hypothesized to be the most widespread siboglinid among seeps on the Arctic shelf. Their absence at PKF could be attributed to environmental factors, including the gravelly seafloor and the geochemical conditions resulting from the presence of oil.

Among epifauna, two prominent groups of polychaete annelids are Sabellida and Onuphidae. We observed Sabellida (including both Sabellidae and Serpulidae) highly abundant, forming dense aggregations near active seepage areas and also farther from the main microbial mat patches, suggesting that bottom currents and access to particulate organic matter may contribute to their high abundance (Bergmann et al., 2011). It's worth noting that other feather duster worms like Sabellida hosting methanotrophic symbionts, were found in Costa Rica's cold seeps with similar abundance to the one we observed at PKF (Goffredi et al., 2020). High densities of Onuphidae have previously been recorded from cold seeps in the Barents Sea (Sen et al., 2018) but did not show an affinity for active seeps, while at PKF, they were more abundant within microbial mats. The onuphid genus *Nothria,* considered a predator or scavenger (Budaeva et al., 2016), has a clear preference for bacterial mats at PKF, most likely related to an increased abundance of prey.

The cold seep sediment infauna has historically received less attention compared to megafauna. Analyses of sediment infauna from Gulf of Mexico oil seeps (Green Canyon, 700 m) and Santa Barbara (Isla Vista Seep, 16 m) revealed communities with high density but low species richness (Robinson et al., 2004). In our study, the key difference in infauna between oil-impregnated sediments and background samples was the reduced diversity of taxa in nematodes, foraminifera, and polychaetes in oily samples. Polychaetes displayed a clear difference in species composition between microbial mats and reference sites. Bacterial mat samples primarily contained taxa tolerant to sulphidic conditions, such as *Capitella* sp. and *Ophryotrocha* sp. (Gamenick et al., 1998). These genera are known to inhabit hydrothermal vents, cold seeps, and organically enriched sediments in shallow water (Gamenick et al., 1998; Thornhill et al., 2012; Holte and Oug, 1996).

Regarding nematode communities, comprehensive studies with high taxonomic resolution have been limited (Spies and Davis, 1979), making comparing our results with other natural oil seep sites challenging. However, unlike other infauna groups, nematode abundance remained consistent across all the investigated microhabitats. Opportunistic species can thrive under unfavorable conditions, such as high hydrogen sulfide and low oxygen levels, by responding to increased food availability from chemosynthetic sources like microbial mats, a trait observed in various seep environments (Vanreusel et al., 2010). Nevertheless, our observations revealed certain similarities between our site and others in the region. For instance, we noted the presence of *Halomonhystera* cf. *disjuncta*, which also dominated microbial mats at the Haakon Mosby Mud Volcano (HMMV), comprising up to 98 % of the nematode fauna (Van Gaever et al., 2006). Habitat/food preferences can additionally help explain the occurrence of observed tolerant taxa in relatively high abundances. For example, specific traits, such as a longer and thinner body shape, as observed in Linhomoidae nematodes, have been hypothesized to be favorable for life under reduced sediment conditions, allowing larger mobility within the sediment column when searching for oxygen pockets (Lampadariou et al., 2013). Another noteworthy adaptation in the present study and in HMMV is the ovoviviparous reproduction mode observed in the Monhysterid nematode *H.* cf. *disjuncta* (Fig. 4). This adaptation allows juveniles to develop internally and migrate within sediment pores to higher oxygen spaces, escaping the toxic effects of high hydrogen sulfide concentrations (Van Gaever et al., 2006).

Foraminifera are less abundant within microbial mats, emitting oil sites with respect to the background. The lack of agglutinated foraminifera in samples with high methane and oil concentrations confirms previous observations at Hydrate Ridge (Heinz et al., 2005), Blake Ridge (Panieri and Sen Gupta, 2008), and the Arctic Ocean (Dessandier et al., 2019). This group of foraminifera that build the text with foreign particles held together by an organic cement seems incapable of tolerating the harsh geochemical conditions present within seeps. When there is methane seepage, the sediments above the SMTZ are enriched in hydrogen sulfide and depleted in methane, which can lead to a toxic environment for the benthic foraminifera (Bernhard et al., 2001; Dessandier et al., 2019) and other organisms. The group that appears to be adapted to thrive under such harsh conditions is monothalamids. A previous study (Bernhard, 1996) illustrated an association between *Allogromia* sp. and filaments of the large, sulfide-oxidizing bacterium *Beggiatoa* that occur near oxic/anoxic interfaces. These observations, and the occurrence of some species in subsurface sediments, suggest that certain monothalamids can, at least, withstand some degree of dysoxia

(Gooday, 2002). In microbial mats, in addition to oil and high concentrations of hydrogen sulfide, pCO_2 due to methane oxidation close to the seafloor may also represent an obstacle for infaunal organisms, particularly those with calcareous shells. For example, high pCO_2 can control calcification or dissolve the calcareous tests in foraminifera in cold seeps (Dessandier et al., 2019; Herguera et al., 2014). Visual observations of fossil benthic foraminifera shells from PKF revealed altered shells with noticeable dissolution features, confirming previous observations from methane seep site (Panieri et al., 2016; Schneider et al., 2017). Another evidence of dissolution is the numerous inner organic linings of foraminifera found in samples impregnated by oil. The organic linings of the inner wall of foraminifera are marine palynomorphs that, due to their fragility, are very difficult to find (Boonstra et al., 2015). The inner organic linings observed from microbial mats may result from species transported from nearby areas that fell on bacterial mats, with calcite shells then becoming dissolved. Yet, because methane emissions are episodic and have strong spatial and short-period temporal variations, it is more plausible that the calcite shells were already present and that newly established emission points created conditions for the shells to dissolve.

In general, the faunal communities of the PKF oil-dominated seep are similar to what is known from shallow-water Arctic seeps without the presence of oil (Panieri et al., 2017; Sahling et al., 2014; Sen et al., 2020; Zajączkowski et al., 2010), suggesting that fauna already adapted to the environmental conditions at cold seeps can tolerate the presence of oil as well. This matches findings from oil seeps in the Gulf of Mexico, where typical seep megafauna, such as *Lamellibrachia* tubeworms and *Bathymodiolus* bivalves, are also found in oil-influenced seeps (MacDonald et al., 2004). However, future studies with higher taxonomic resolution and quantitative community analyses are needed to assess the potential added impact of oil on the community composition of cold seeps in the Arctic.

5. Conclusions and future directions

Our results represent an integrated, multidisciplinary characterization of a recently discovered Arctic oil seep site offshore Prins Karls Forland (80–100 m water depth) based on multisource data from remote sensing, geochemistry, and biology. The oil slick at PKF originates from the seep beneath and consists of severely biodegraded oil from an unknown source rock at depth, with a Tertiary age or younger, also confirmed by the dominant biodegraded thermogenic methane. Interestingly, no oil with such a young age has previously been reported from this part of the Arctic or the North Atlantic. The U/Th dating of carbonate crusts yields an age of 18.5 ± 1.6 ka, indicating protracted activity for this seepage system since the Late Pleistocene as a response to post-glacial climate warming and deglaciation. The ROV imaging shows methane and oil bubbles seeping from the clustering of bacterial patches that are preferentially aligned South-East to North-West, suggesting emissions from fractures, in agreement with the proximity to the seafloor of the regional unconformity separating the FMC from the underlying eroded bedrock along the Hornsund fault system. Biological investigations show that the faunal communities are a mix of typical fauna found in high latitude areas and taxa adapted to reducing environments. Remarkably, oil-impregnated sediments that might seem to be an inhospitable environment are colonized by abundant infauna organisms.

Ecosystems within hydrocarbon seep sites deserve particular attention in marine protection area planning evaluations. Such ecosystems host specific fauna and offer food resources to background fauna, including potential species of economic importance (e.g., fish). Seep sites are also ideal for oil degradation studies and identifying potential biotechnological resources of economic interest. The spatial dimension of ecosystems as the one identified in PKF is unknown in the Arctic. They represent an enormous carbon source that cannot be ignored when estimating the C cycle in this region.

The multidisciplinary approach of this paper demonstrates a new state-of-the-art for researching Arctic ecosystems on the seafloor. Moreover, the proximity of the PKF oil seep site to research facilities and infrastructure within Longyearbyen on Svalbard, makes it an easily accessible natural laboratory to understand better future oil spill processes within the water column, on the sea surface, and under sea ice.

Whether or not ocean warming will impact oil seepage within the shallow Arctic, as is understood for methane, is currently difficult to predict. Yet, we confirmed that satellite imagery played a crucial role in targeting study areas and quantifying processes (Yang et al., 2013), and in outlining study objectives, which were then pursued by our research through the organization of a multidisciplinary oceanographic expedition.

Funding

Norwegian Research Council, project number 287869 (GP, CA, SPR, FV, LF, AS, DK, SB), Norwegian Research Council, project number 223259 (GP, SB), Norwegian Research Council project number 315427 (RS, FV, IHS), Norwegian Biodiversity Information Centre, the Norwegian Taxonomy Initiative, project "Fauna of hydrothermal vents and cold seeps in Norwegian waters", project number 70184243 (MHE). SPR acknowledges support from FCT/MCTES through the CEEC contract 475 (CEECIND/00758/2017) and grants UIDP/50017/2020, UIDB/50017/2020 and LA/P/0094/2020476 to CESAM at the University of Aveiro.

CRediT authorship contribution statement

Giuliana Panieri: Conceptualization, Methodology, Investigation, Visualization, Supervision, Writing – original draft, Writing – review & editing. **Claudio Argentino:** Methodology, Investigation, Visualization, Writing – original draft, Writing – review & editing. **Sofia P. Ramalho:** Methodology, Investigation, Visualization, Writing – original draft, Writing – review & editing. **Francesca Vulcano:** Methodology, Investigation, Visualization, Writing – original draft, Writing – review & editing. **Alessandra Savini:** Methodology, Investigation, Visualization, Writing – original draft, Writing – review & editing. **Luca Fallati:** Methodology, Investigation, Visualization, Writing – review & editing. **Trond Brekke:** Methodology, Writing – review & editing. **Giulia Galimberti:** Methodology, Investigation, Writing – review & editing. **Federica Riva:** Methodology, Investigation, Writing – review & editing. **João Balsa:** Methodology, Investigation, Writing – review & editing. **Mari H. Eilertsen:** Methodology, Investigation, Writing – review & editing. **Runar Stokke:** Methodology, Investigation, Writing – review & editing. **Ida H. Steen:** Methodology, Investigation, Writing – review & editing. **Diana Sahy:** Methodology, Investigation, Writing – review & editing. **Dimitri Kalenitchenko:** Methodology, Investigation, Writing – review & editing. **Stefan Büenz:** Methodology, Investigation, Writing – review & editing. **Rune Mattingsdal:** Methodology, Investigation, Writing – original draft, Writing – review & editing.

Declaration of competing interest

All authors declare they have no competing interests.

Data availability

All data are in the main text or the supplementary materials. The data are also available at https://doi.org/10.18710/65WIJO, DataverseNO, V1 https://dataverse.no.

Acknowledgments

The Norwegian Research Council supported our research through project AKMA, Advancing Knowledge of Methane in the Arctic (project number 287869) and the Centre for Arctic Gas Hydrate, Environment

and Climate (project number 223259). We thank Carole Petetin for the artwork, the lab staff at the Arctic University of Norway, the Norwegian Petroleum Directorate (for financial support for geochemical analysis and interpretation), Marte L. B. Klemetsrud in the Department of Biological Sciences at the University of Bergen and Jon A. Kongsrud at the University Museum of Bergen for help with macrofauna sample identification, and Ove Njøten at the Norwegian Coastal Administration for making us aware of oil slicks outside Prins Karls Forland, observed on radar satellite images. All data needed to evaluate the conclusions are present in the paper and the Supplementary Materials.

Appendix A. Supplementary data

Supplementary data to this article can be found online at https://doi.org/10.1016/j.scitotenv.2023.167788.

References

Agisoft, 2018. Agisoft photoscan user manual. Prof. Edit. Ver. 1, 4.
Alfred R. Loeblich, H.T., 1988. Foraminiferal Genera and Their Classification, XL, 2031 pp.
Alpers, W., Holt, B., Zeng, K., 2017. Oil spill detection by imaging radars: challenges and pitfalls. Remote Sens. Environ. 201, 133–147.
Altabet, M., 2005. Isotopic tracers of the marine nitrogen cycle: present and past. In: Volkman, J.K. (Ed.), Marine Organic Matter: Biomarkers, Isotopes and DNA. Springer, Berlin, pp. 251–293.
Andreassen, K., et al., 2017. Massive blow-out craters formed by hydrate-controlled methane expulsion from the Arctic seafloor. Science 356 (6341), 948–953.
Barnes, R.O., Goldberg, E.D., 1976. Methane production and consumption in anoxic marine sediments. Geology 4 (5), 297–300.
Bergmann, M., et al., 2011. Megafaunal assemblages from two shelf stations west of Svalbard. Mar. Biol. Res. 7 (6), 525–539.
Berndt, C., et al., 2014. Temporal constraints on hydrate-controlled methane seepage off Svalbard. Science 343, 284–287.
Bernhard, J., 1996. Microaerophilic and facultative anaerobic benthic foraminifera: a review of experimental and ultrastructural evidence. Rev. Paléobiol. 15 (1), 261–275.
Bernhard, J.M., Buck, K.R., Barry, J.P., 2001. Monterey Bay cold-seep biota: assemblages, abundance, and ultrastructure of living foraminifera. Deep-Sea Res. I Oceanogr. Res. Pap. 48 (10), 2233–2249.
Bezerra, T.N., Deprez, T., Eisendle, U., Hodda, M., Holovachov, O., Leduc, D., Mokievsky, V., Peña Santiago, R., Pérez-García, J.A., Sharma, J., Smol, N., Tchesunov, A., Vanreusel, A., Venekey, V., Zhao, Z., 2022. Nemys, world database of nematodes. In: Bánki, O., Roskov, Y., Döring, M., Ower, G., Vandepitte, L., Hobern, D., Remsen, D., Schalk, P., DeWalt, R.E., Keping, M., Miller, J., Orrell, T., Aalbu, R., Adlard, R., Adriaenssens, E.M., Aedo, C., Aescht, E., Akkari, N., Alexander, S., et al. (Eds.), Catalogue of Life Checklist (ver. (08/2022)).
Boonstra, M., Ramos, M., Lammertsma, E.I., Antoine, P.-O., Hoorn, C., 2015. Marine connections of Amazonia: evidence from foraminifera and dinoflagellate cysts (early to middle Miocene, Colombia/Peru). Palaeogeogr. Palaeoclimatol. Palaeoecol. 417, 176–194.
Budaeva, N., Schepetov, D., Zanol, J., Neretina, T., Willassen, E., 2016. When molecules support morphology: phylogenetic reconstruction of the family Onuphidae (Eunicida, Annelida) based on 16S rDNA and 18S rDNA. Mol. Phylogenet. Evol. 94 (Pt B), 791–801.
Bünz, S., Panieri, G., 2021. **CAGE-21-1. AKMA-AKER-GReAT** cruise report. Institution: UiT, The Arctic University of Norway. https://hdl.handle.net/11250/2735220.
Cremiere, A., et al., 2016. Timescales of methane seepage on the Norwegian margin following collapse of the Scandinavian Ice Sheet. Nat. Commun. 7 (11509), 1–10.
Dessandier, P.-A., Borrelli, C., Kalenitchenko, D., Panieri, G., 2019. Benthic foraminifera in Arctic methane hydrate bearing sediments. Front. Mar. Sci. 6.
Dessandier, P.-A., Knies, J., Plaza-Faverola, A., Labrousse, C., Renoult, M., 2021. Ice-sheet melt drove methane emissions in the Arctic during the last two interglacials. Geology 49, 5. https://doi.org/10.1130/G48580.1.
Dong, Y., Liu, Y., Hu, C., MacDonald, I.R., Lu, Y., 2022. Chronic oiling in global oceans. Science 376 (6599), 1300–1304.
Du, M., et al., 2014. High resolution measurements of methane and carbon dioxide in surface waters over a natural seep reveal dynamics of dissolved phase air–sea flux. Environ. Sci. Technol. 48 (17), 10165–10173.
Emil Ruff, S., 2020. Microbial communities and metabolisms at hydrocarbon seeps. In: Teske, A., Carvalho, V. (Eds.), Marine Hydrocarbon Seeps: Microbiology and Biogeochemistry of a Global Marine Habitat. Springer International Publishing, Cham, pp. 1–19.
Fallati, L., et al., 2020. Multi-temporal UAV data and Object-Based Image Analysis (OBIA) for estimation of substrate changes in a post-bleaching scenario on a Maldivian reef. Remote Sens. 12 (13), 2093.
Fiscella, B., Giancaspro, A., Nirchio, F., Pavese, P., Trivero, P., 2000. Oil spill detection using marine SAR images. Int. J. Remote Sens. 21 (18), 3561–3566.
Gamenick, I., Vismann, B., Grieshaber, M., Giere, O., 1998. Ecophysiological differentiation of Capitella capitata (Polychaeta). Sibling species from different sulfidic habitats. Mar. Ecol. Prog. Ser. 175, 155–166.
Garcia-Pineda, MacDonald, I.R., Li, X., Jackson, C.R., Pichel, W.G., 2013. Oil spill mapping and measurement in the Gulf of Mexico with Textural Classifier Neural Network Algorithm (TCNNA). IEEE J. Sel. Top. Appl. Earth Obs. Remote Sens. 6, 2517–2525. https://doi.org/10.1109/JSTARS.2013.2244061.
Gebruk, A.V., et al., 2003. Methane seep community of the Håkon Mosby mud volcano (the Norwegian Sea): composition and trophic aspects. Sarsia 88 (6), 394–403.
Goffredi, S.K., et al., 2020. Methanotrophic bacterial symbionts fuel dense populations of deep-sea feather duster worms (Sabellida, Annelida) and extend the spatial influence of methane seepage. Sci Adv. 6 (14), eaay8562 https://doi.org/10.1126/sciadv.aay8562. Apr 3; PMID: 32284974; PMCID: PMC7124940.
Gooday, A.J., 2002. Organic-walled Allogromiids: aspects of their occurrence, diversity and ecology in marine habitats. J. Foraminifer. Res. 32 (4), 384–399.
Gruber-Vodicka, H.R., et al., 2019. Two intracellular and cell type-specific bacterial symbionts in the placozoan Trichoplax H2. Nat. Microbiol. 4 (9), 1465–1474.
Gunnarsson, B., 2021. Recent ship traffic and developing shipping trends on the Northern Sea Route—policy implications for future arctic shipping. Mar. Policy 124, 104369.
Head, I.M., Jones, D.M., Larter, S.R., 2003. Biological activity in the deep subsurface and the origin of heavy oil. Nature 426 (6964), 344–352.
Heinz, P., Sommer, S., Pfannkuche, O., Hemleben, C., 2005. Living benthic foraminifera in sediments influenced by gas hydrates at the Cascadia convergent margin, NE Pacific. Mar. Ecol. Prog. Ser. 304, 77–89.
Heip, C.H.R., Vincx, M., Vranken, G., 1985. The ecology of marine nematodes. Oceanogr. Mar. Biol. 23, 399–489.
Herguera, J.C., Paull, C.K., Perez, E., Ussler III, W., Peltzer, E., 2014. Limits to the sensitivity of living benthic foraminifera to pore water carbon isotope anomalies in methane vent environments. Paleoceanography 29 (3), 273–289.
Higgins, R.P., Thiel, H., 1988. Introduction to the Study of Meiofauna. Smithsonian Institution Press Washington, D.C., Washington, D.C.
Holba, A.G., et al., 1998. Application of 24-norcholestanes for constraining source age of petroleum. Org. Geochem. 29 (5), 1269–1283.
Holte, B., Oug, E., 1996. Soft-bottom macrofauna and responses to organic enrichment in the subarctic wates of Tromsø, northern Norway. J. Sea Res. 36 (3), 227–237.
Hu, Y., et al., 2020. A prominent isotopic fingerprint of nitrogen uptake by anaerobic methanotrophic archaea. Chem. Geol. 558, 119972.
Ishizawa, M., et al., 2019. Analysis of atmospheric CH4 in Canadian Arctic and estimation of the regional CH4 fluxes. Atmos. Chem. Phys. 19 (7), 4637–4658.
Ivanov, A.Y., 2019. Remote sensing detection and analysis of oil seeps in the Caspian Sea and the Barents Sea. J. Oceanol. Res. 47 (5), 52–64. https://doi.org/10.29006/1564-2291.JOR-2019.47(5).4.
Kim, S.-T., O'Neil, J.R., Hillaire-Marcel, C., Mucci, A., 2007. Oxygen isotope fractionation between synthetic aragonite and water: influence of temperature and Mg2+ concentration. Geochim. Cosmochim. Acta 71 (19), 4704–4715.
Knies, J., Mann, U., 2002. Depositional environment and source rock potential of Miocene strata from the central Fram Strait: introduction of a new computing tool for simulating organic facies variations. Mar. Pet. Geol. 19 (7), 811–828.
Knies, J., Martinez, P., 2009. Geochemistry of surface sediment samples from the western Barents Sea region, supplement to: Knies, J; Martinez, P (2009): organic matter sedimentation in the western Barents Sea region: Terrestrial and marine contribution based on isotopic composition and organic nitrogen content. Nor. J. Geol. 89, 79–89. http://www.geologi.no/images/njg/2009/1-2/Knies_print.pdf (PANGAEA).
Knies, J., et al., 2018. Modelling persistent methane seepage offshore western Svalbard since early Pleistocene. Mar. Pet. Geol. 91, 800–811.
Kvenvolden, K.A., Cooper, C.K., 2003. Natural seepage of crude oil into the marine environment. Geo-Mar. Lett. 23 (3), 140–146.
LaMontagne, M.G., Leifer, I., Bergmann, S., Van De Werfhorst, L.C., Holden, P.A., 2004. Bacterial diversity in marine hydrocarbon seep sediments. Environ. Microbiol. 6 (8), 799–808.
Lampadariou, N., Kalogeropoulou, V., Sevastou, K., Keklikoglou, K., Sarrazin, J., 2013. Influence of chemosynthetic ecosystems on nematode community structure and biomass in the deep eastern Mediterranean Sea. Biogeosciences 10 (8), 5381–5398.
Landvik, J.Y., et al., 2005. Rethinking late Weichselian ice-sheet dynamics in coastal NW Svalbard. Boreas 34 (1), 7–24.
Lehmann, M.F., Bernasconi, S.M., Barbieri, A., McKenzie, J.A., 2002. Preservation of organic matter and alteration of its carbon and nitrogen isotope composition during simulated and in situ early sedimentary diagenesis. Geochim. Cosmochim. Acta 66 (20), 3573–3584.
Leifer, I., 2019. A synthesis review of emissions and fates for the coal oil point marine hydrocarbon seep field and California marine seepage. Geofluids 2019, 4724587.
Leifer, I., Patro, R.K., 2002. The bubble mechanism for methane transport from the shallow sea bed to the surface: a review and sensitivity study. Cont. Shelf Res. 22 (16), 2409–2428.
Levin, L.A., et al., 2016. Hydrothermal vents and methane seeps: rethinking the sphere of influence. Front. Mar. Sci. 3 (72).
Lewis, A., 2007. CURRENT STATUS OF THE BAOAC (BONN AGREEMENT OIL APPEARANCE CODE). A Report to the Netherlands North Sea Agency Directie Noordzee by Alun Lewis Oil Spill Consultant. 19.
Lien, Ø.F., Hjelstuen, B.O., Zhang, X., Sejrup, H.P., 2022. Late Plio-Pleistocene evolution of the Eurasian Ice Sheets inferred from sediment input along the northeastern Atlantic continental margin. Quat. Sci. Rev. 282, 107433.
Lim, A., et al., 2020. Influence of benthic currents on cold-water coral habitats: a combined benthic monitoring and 3D photogrammetric investigation. Sci. Rep. 10 (1), 19433.
Liu, Y.-F., et al., 2019. Anaerobic hydrocarbon degradation in candidate phylum 'Atribacteria' (JS1) inferred from genomics. ISME J. 13 (9), 2377–2390.
MacDonald, I.R., et al., 2002. Transfer of hydrocarbons from natural seeps to the water column and atmosphere. Geofluids 2 (2), 95–107.

MacDonald, I.R., et al., 2004. Asphalt volcanism and chemosynthetic life in the Campeche Knolls, Gulf of Mexico. Science 304 (5673), 999–1002.
Marcon, Y., Purser, A., 2017. PAPARA(ZZ)I: an open-source software interface for annotating photographs of the deep-sea. SoftwareX 6, 69–80.
Migliaccio, M., Nunziata, F., Buono, A., 2015. SAR polarimetry for sea oil slick observation. Int. J. Remote Sens. 36 (12), 3243–3273.
Milkov, A.V., Etiope, G., 2018. Revised genetic diagrams for natural gases based on a global dataset of >20,000 samples. Org. Geochem. 125, 109–120.
Mityagina, M., Lavrova, O., 2022. Satellite survey of offshore oil seep sites in the Caspian Sea. Remote Sens. 14 (3), 525.
Ottesen, D., et al., 2008. Submarine landforms characteristic of glacier surges in two Spitsbergen fjords. Quat. Sci. Rev. 27 (15), 1583–1599.
Pachiadaki, M.G., Kallionaki, A., Dählmann, A., De Lange, G.J., Kormas, K.A., 2011. Diversity and spatial distribution of prokaryotic communities along a sediment vertical profile of a deep-sea mud volcano. Microb. Ecol. 62 (3), 655–668.
Panieri, G., Sen Gupta, B.K., 2008. Benthic Foraminifera of the Blake Ridge hydrate mound, Western North Atlantic Ocean. Mar. Micropaleontol. 66 (2), 91–102.
Panieri, G., et al., 2016. Diagenetic Mg-calcite overgrowths on foraminiferal tests in the vicinity of methane seeps. Earth Planet. Sci. Lett. 458, 203–212.
Panieri, G., et al., 2017. An integrated view of the methane system in the pockmarks at Vestnesa Ridge, 79°N. Mar. Geol. 390, 282–300.
Panieri, G., et al., 2022. CAGE-22-2 Scientific Cruise Report. AKMA 2/Ocean Senses, UiT &#8211. The Arctic University of Norway.
Panieri, G., Knies, J., Vadakkepuliyambatta, S., Lee, A.L., Schubert, C.J., 2023. Commun. Earth Environ. 4 (1), 109. https://doi.org/10.1038/s43247-023-00772-y.
Parapar, J., Moreira, J., Helgason, G.V., 2011. Distribution and diversity of the Opheliidae (Annelida, Polychaeta) on the continental shelf and slope of Iceland, with a review of the genus Ophelina in northeast Atlantic waters and description of two new species. Org. Divers. Evol. 11 (2), 83.
Pavel Serov, R.M., Winsborrow, Monica, Patton, Henry, Andreassen, Karin, 2022. Widespread natural methane and oil leakage from sub-marine Arctic reservoirs. In: PREPRINT (Version 1) Available at Research Square.
Perdue, E.M., Koprivnjak, J.-F., 2007. Using the C/N ratio to estimate terrigenous inputs of organic matter to aquatic environments. Estuar. Coast. Shelf Sci. 73 (1), 65–72.
Peters, K.E., Peters, K.E., Walters, C.C., Moldowan, J., 2005. The Biomarker Guide, 1. Cambridge university press.
Pitusi, Søreide, J.E., Hassett, B.T., Marquardt, M., Andreasen, M.H., 2021. The occurrence of Nematoda in coastal sea ice on Svalbard (European Arctic) determined with the 18S small subunit rRNA gene. Polar Biol. 44 (6), 1153–1162. https://doi.org/10.1007/s00300-021-02863-y.
Platt, H.M., Warwick, R.M., 1988. Free-living marine nematodes part II, British Chromadorids. Synopses of the British Fauna (new series). In: Kermack, Doris M., Barnes, R.S.K. (Eds.), Published for the Linnean Society of London and the Estuarine and Brackish-Water Sciences Association by E.J. Brill / Dr W. Backhuys.
Price, D.M., et al., 2019. Using 3D photogrammetry from ROV video to quantify cold-water coral reef structural complexity and investigate its influence on biodiversity and community assemblage. Coral Reefs 38 (5), 1007–1021.
Rabus, R., et al., 2016. Anaerobic microbial degradation of hydrocarbons: from enzymatic reactions to the environment. J. Mol. Microbiol. Biotechnol. 26 (1–3), 5–28.
Robinson, C.A., Bernhard, J.M., Levin, L.A., Mendoza, G.F., Blanks, J.K., 2004. Surficial hydrocarbon seep infauna from the Blake Ridge (Atlantic Ocean, 2150 m) and the Gulf of Mexico (690–2240 m). Mar. Ecol. 25 (4), 313–336.
Sahling, H., et al., 2014. Gas emissions at the continental margin west of Svalbard: mapping, sampling, and quantification. Biogeosciences 11 (21), 6029–6046.
Savvichev, A.S., et al., 2018. Methane as an organic matter source and the trophic basis of a Laptev Sea cold seep microbial community. Geomicrobiol J. 35 (5), 411–423.
Schneider, A., Cremiere, A., Panieri, G., Lepland, A., Knies, J., 2017. Diagenetic alteration of benthic foraminifera from a methane seep site on Vestnesa Ridge (NW Svalbard). Deep-Sea Res. I Oceanogr. Res. Pap. 123, 22–34.
Schneider, A., et al., 2018. Methane seepage at Vestnesa Ridge (NW Svalbard) since the last glacial maximum. Quat. Sci. Rev. 193, 98–117.
Seinhorst, J.W., 1959. A rapid method for the transfer of nematodes from fixative to anhydrous glycerin. Nematologica 4 (1), 67–69.
Sen, A., et al., 2018. Geophysical and geochemical controls on the megafaunal community of a high Arctic cold seep. Biogeosciences 15 (14), 4533–4559.
Sen, A., Didriksen, A., Hourdez, S., Svenning, M.M., Rasmussen, T.L., 2020. Frenulate siboglinids at high Arctic methane seeps and insight into high latitude frenulate distribution. Ecol. Evol. 10 (3), 1339–1351.
Serov, P., et al., 2017. Postglacial response of Arctic Ocean gas hydrates to climatic amelioration. Proc. Natl. Acad. Sci. U. S. A. 114 (24), 6215–6220.
Serov, P., Mattingsdal, R., Winsborrow, M., Patton, H., Andreassen, K., 2023. Widespread natural methane and oil leakage from sub-marine Arctic reservoirs. Nat. Commun. 14 (1), 1782.
Speelman, E.N., et al., 2009. The Eocene Arctic Azolla bloom: environmental conditions, productivity and carbon drawdown. Geobiology 7 (2), 155–170.
Spies, R.B., Davis, P.H., 1979. The infaunal benthos of a natural oil seep in the Santa Barbara channel. Mar. Biol. 50 (3), 227–237.
Steinbach, J., et al., 2021. Source apportionment of methane escaping the subsea permafrost system in the outer Eurasian Arctic Shelf. Proc. Natl. Acad. Sci. 118 (10), e2019672118.
Stokke, R., Roalkvam, I., Lanzen, A., Haflidason, H., Steen, I.H., 2012. Integrated metagenomic and metaproteomic analyses of an ANME-1-dominated community in marine cold seep sediments. Environ. Microbiol. 14 (5), 1333–1346.
Thornhill, D.J., et al., 2012. Adaptive radiation in extremophilic Dorvilleidae (Annelida): diversification of a single colonizer or multiple independent lineages? Ecol. Evol. 2 (8), 1958–1970.
Van Gaever, S., Moodley, L., De Beer, D., Vanreusel, A., 2006. Meiobenthos at the Arctic Håkon Mosby Mud Volcano, with a parental-caring nematode thriving in sulphide-rich sediments. Mar. Ecol. Prog. Ser. 321, 143–155.
Vanreusel, A., et al., 2010. The contribution of deep-sea macrohabitat heterogeneity to global nematode diversity. Mar. Ecol. 31 (1), 6–20.
Vigneron, A., et al., 2017. Comparative metagenomics of hydrocarbon and methane seeps of the Gulf of Mexico. Sci. Rep. 7 (1), 16015.
Warwick, R.M., Platt, H.M., Somerfield, P.J., 1998. Free-living Marine Nematodes Part III. Monhysterids. Synopses of the British Fauna (New Series), 53. Field Studies Council: Shrewsbury. ISBN 1-85153-260-9., 296.
Weiss, H.M., et al., 2000. NIGOGA - The Norwegian Industry Guide to Organic Geochemical Analyses [online]. Edition 4.0 Published by Norsk Hydro, Statoil, Geolab Nor, SINTEF Petroleum Research and the Norwegian Petroleum Directorate. 102 pp [cited 27.09.2022]. Available from World Wide Web. https://www.npd.no/en/regulations/reporting_and_applications/wells/geochemical-analyses-guide/.
Wenger, L.M., Davis, C.L., Isaksen, G.H., 2002. Multiple controls on petroleum biodegradation and impact on oil quality. SPE Reserv. Eval. Eng. 5 (05), 375–383.
Whiticar, M.J., 1999. Carbon and hydrogen isotope systematics of bacterial formation and oxidation of methane. Chem. Geol. 161 (1), 291–314.
Yang, J., et al., 2013. The role of satellite remote sensing in climate change studies. Nat. Clim. Chang. 3 (10), 875–883.
Zajączkowski, M., Szczuciński, W., Plessen, B., Jernas, P., 2010. Benthic foraminifera in Hornsund, Svalbard: implications for paleoenvironmental reconstructions. Pol. Polar Res. 31 (4), 349–375. https://doi.org/10.2478/v10183-010-0010-4.